

Article

Spectral Characterization and Identification of Natural and Regenerated Leather Based on Hyperspectral Imaging System

Qijin Hou ^{1,2} , Xiaoke Jin ^{1,2}, Yingjie Qiu ^{1,2}, Zeya Zhou ^{1,2}, Huifang Zhang ³, Jingjing Jiang ⁴, Wei Tian ^{1,2,*} and Chengyan Zhu ^{1,2,*}

¹ College of Textile Science and Engineering (International Institute of Silk), Zhejiang Sci-Tech University, Hangzhou 310018, China

² Key Laboratory of Advanced Textile Materials and Manufacturing Technology, Ministry of Education, Zhejiang Sci-Tech University, Hangzhou 310018, China

³ Quality Inspection Institute of Zhejiang Light Industry, Hangzhou 310018, China

⁴ National Textiles and Garment Quality Supervision Inspection Center (Zhejiang Tongxiang), Jiaxing 314502, China

* Correspondence: tianwei_zstu@126.com (W.T.); cyzhu@zstu.edu.cn (C.Z.); Tel.: +86-138-5713-6163 (C.Z.)

Abstract: Currently, the methods to identify leather materials have limitations, and identifying natural leather types is also relatively complex. In this research, the microstructures of four types of mammalian leathers (cattle leather, pig leather, sheep leather, and deer leather), three kinds of reptilian leathers (crocodile leather, lizard leather, and snake leather) and regenerated leather were characterized by scanning electron microscopy. The spectral curves (from 900 to 1700 nm) of these leather samples were extracted using a hyperspectral imaging system, and their spectral characteristics were analyzed. A method of leather identification by the hyperspectral imaging system combined with chemometrics was established. The results showed that the spectral curves of natural and regenerated leather differed in the number, position, and depth of the characteristic peaks, enabling the classification of regenerated leather by comparative analysis with the naked eye. The first-order derivative processing–principal component analysis–discriminant analysis model achieved a 98% correct classification rate, confirming the hyperspectral imaging system’s feasibility in the leather material identification field. We believe that his research is beneficial for the leather industry to understand the classifications scientifically, in order to protect consumer rights and further develop the leather testing industry.

Keywords: hyperspectral imaging; natural leather; regenerated leather; material identification; discriminant analysis



Citation: Hou, Q.; Jin, X.; Qiu, Y.; Zhou, Z.; Zhang, H.; Jiang, J.; Tian, W.; Zhu, C. Spectral Characterization and Identification of Natural and Regenerated Leather Based on Hyperspectral Imaging System. *Coatings* **2023**, *13*, 450. <https://doi.org/10.3390/coatings13020450>

Academic Editors: Rafael Comesaña, Mazeyar Parvinzadeh Gashti and Jiri Militky

Received: 28 November 2022

Revised: 21 January 2023

Accepted: 15 February 2023

Published: 16 February 2023



Copyright: © 2023 by the authors. Licensee MDPI, Basel, Switzerland. This article is an open access article distributed under the terms and conditions of the Creative Commons Attribution (CC BY) license (<https://creativecommons.org/licenses/by/4.0/>).

1. Introduction

Leather products and materials are generally classified as natural leather, artificial leather, and regenerated leather [1]. Among them, natural leather is made from raw animal skin through dehairing and degreasing, acid and alkali treatment, tanning, and finishing, and a series of processes after processing, according to the source of species. Natural leather can be divided into mammals, reptiles, and fish [2] and is highly sought after by consumers due to its excellent performance; natural leather is widely used in apparel, accessories, and home textiles [3,4]. However, the leather market has been chaotic for a long time, and the authenticity of leather products and their labelling properties have always been the focus of attention of consumers, the media, and quality inspection departments [5]. Rare animal skins that are illegally made into luxury leather goods also cause a severe loss of biodiversity [6]. Therefore, the identification of leather materials is also a research hotspot in the leather and textile industry.

Currently, the main identification methods for leather materials are the sensory identification method, chemical analysis, microscopic method, infrared spectroscopy, and DNA

identification method [7–9]. The identification technology of natural and artificial leather is relatively mature [10]. Unfortunately, the method for applying regenerated leather is restricted, and it might be challenging to distinguish between different kinds of natural leather. The identification methods used at this stage have limitations such as a certain degree of sample damage or the inability to meet the efficiency requirements of online testing [11]. In summary, the establishment of an efficient and universal, non-destructive, and accurate digital leather identification method is the key to breaking through the dilemma.

In recent years, image processing technology has become an essential identification technique in various fields [12]. Hyperspectral imaging technology (HIT) is the most representative, which has the advantage of “image and spectrum in one”, with high resolution, continuous channels, more wavebands, and more vital discriminatory ability [13]. HIT originated in remote sensing and has since been widely used in many fields such as feature identification [14,15], environmental monitoring [16,17], agricultural quality inspection [18,19], medical diagnosis [20,21], and criminal forensic investigation [22,23].

In the past few decades, the application of HIT in the textile and leather inspection industries has gained importance, mainly including research on cotton impurity detection, textile material composition identification, textile color measurement, and leather defect detection. Guo et al. used hyperspectral imaging to detect the surface and inner impurities of carded cotton, making a breakthrough in textile inspection through hyperspectral imaging technology [24]. Mustafic et al. solved the problem of lint impurity classification by using hyperspectral imaging technology, with an average classification rate of 90% [25]. Jin et al. established a discriminative analysis model with an accuracy of 96.78% based on hyperspectral imaging technology for the qualitative analysis and identification of textile material components; they confirmed the feasibility of applying hyperspectral imaging technology to the qualitative identification of textile components [26]. Li et al. investigated the hyperspectral data of single-component fabric components and established a classification model with better recognition rate and stability by the local hold algorithm descending and the KNN classifier [27]. Zhang et al. measured 210 cotton swatch colors using a hyperspectral imaging system, and the results showed that the experimental results were reproducible and could be used in color measurement [28]. Chen et al. proposed a hyperspectral leather defect detection algorithm capable of automated grading based on hyperspectral imaging technology for the surface detection of blue wet leather defects [29]. However, there is little related research on identifying leather materials by hyperspectral imaging technology, and researchers have not profoundly explored the potential of combining the two.

This study investigated the viability of completing leather material identification through a hyperspectral imaging system, which has rarely been used before. The natural and regenerated leather spectral characteristics were analyzed by the original reflection spectra. In addition, a leather material identification method based on a hyperspectral imaging system and chemometrics was established, confirming the feasibility of the application and development of hyperspectral imaging technology in the field of leather material identification as it is a digital and non-destructive approach for leather classification. This research is essential for advancing the leather testing business and safeguarding consumer rights in the leather market.

2. Materials and Methods

2.1. Materials

Different kinds of mammalian, reptilian, and regenerated leather sources were used for the experiments. The sources of the samples and their identification were provided by the Quality Inspection Institute of Zhejiang Light Industry (Hangzhou, China), and the leather samples are shown in Figure 1. The selected regenerated leather, also known as “leather bran paper”, was leather fiber cardboard.



Figure 1. The leather samples.

2.2. Structure Characterization by Scanning Electron Microscopy (SEM)

The instrument used in this experiment was a JSM-5610LV tungsten filament scanning electron microscope from Nippon Electron (Tokyo, Japan). The leather samples were cut to the appropriate size for the SEM carrier table, and then the cut leather sample pieces were fixed in order on the carrier table with conductive adhesive. The order of the various leather samples was recorded for subsequent observation. The carrier table was placed in the coater (JFC-3000FC), and the 20 mA current was selected for gold spraying for 60 s. The plated samples were placed in the sample compartment, and the cross-sections of the leather samples were observed by scanning electron microscopy. The cross-sectional SEM image of the leather sample was obtained by selecting the photographed area and adjusting the magnification, focus, and dispersion.

2.3. Experimental Instrumentation and Processing Software

The acquisition of the spectral data of the leather samples was carried out by a push-scan NIR hyperspectral imaging system (Wuling Optical Co. Ltd., Taiwan, China), as shown in Figure 2, whose core components were as follows: NIR spectrometer (ImSpector N17E, China), spectral range from 890 to 1728 nm, spectral resolution 3.27 nm; image element number 320×320 pixels, camera spatial resolution $273 \mu\text{m}$; S31/f2.0 camera lens; 150 W halogen light source; step sample moving table (IRCP0076-1COMB, China); computer equipped with Spectral-image imaging software (version 1.3) and HIS-Analyzer analysis software (version 2.4).

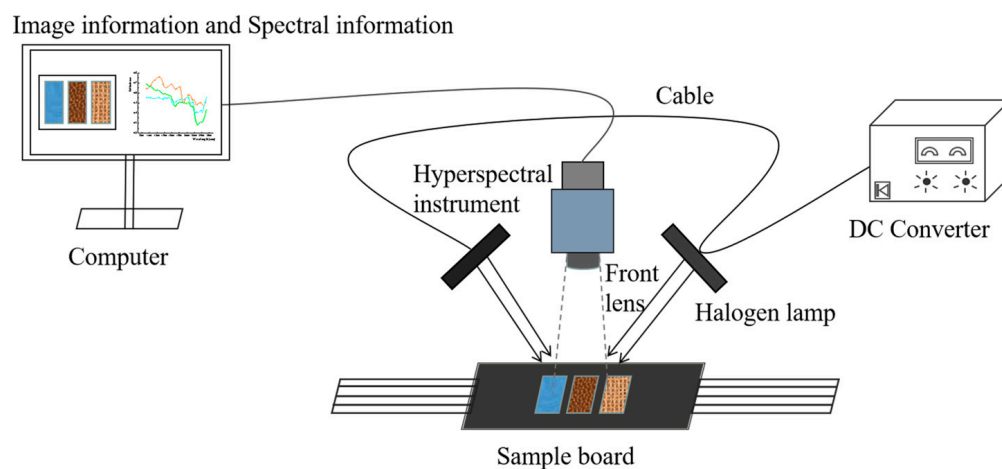


Figure 2. Schematic diagram of the hyperspectral imaging system.

The subsequent processing software used included ENVI 5.3 (extraction of spectral information), MATLAB R2019b (spectral transformation processing), Origin 2018 (plotting and data analysis), and IBM SPSS Statistics 27 (discriminant analysis).

2.4. Hyperspectral Image Acquisition and Data Pre-Processing

The lights were turned on in advance to warm up for 10 min, and the hyperspectral image acquisition software was started to observe whether the camera connection was correct. The leather samples were laid flat on the carrier table in order of the rules of the species, keeping a certain distance between the samples to prevent any influence due to mutual overlap. The relevant parameters were set to ensure that complete and clear images of the samples were obtained such as the exposure time, the distance between the lens and the sample, the camera focal length, and light source intensity. Moreover, the average digital quantization value (DN) in the standard calibration white board was adjusted to approximately 80% (3200) of the maximum DN value (4096) stored in the CCD. The moving speed of the stepper stage was adjusted to 3.75 mm/s, so that the acquired sample images would not be distorted or deformed, and the experimental efficiency would be maximized. The entire experiment was conducted in a dark box to prevent interference from external light, and spectral data measurements of a standard white board and dark current were performed before sample image acquisition. The images were acquired using the flesh side of the leather for the experiments to circumvent the effects of leather coating and processing.

The presence of a dark current in the hyperspectral imager and the noise generated by the uneven light intensity distribution impacted the leather sample images. In addition, the spectral data in the hyperspectral images were stored in the form of DN values for each pixel point, which represented the light intensity of each pixel point and needed to be converted into reflectance for further analysis. Therefore, black and white board correction pre-processing is necessary, and the equation is as follows:

$$R_{ref} = \frac{DN_{raw} - DN_{dark}}{DN_{white} - DN_{dark}} \quad (1)$$

where R_{ref} is the corrected hyperspectral image; DN_{raw} is the original hyperspectral image; DN_{white} is the calibration image of the standard white board; DN_{dark} is the calibration image of the dark current.

The hyperspectral images of the leather samples corrected by the black and white board were selected as the region of interest (ROI), and the spectra of all pixels in the region were averaged to obtain a total of 150 pixel \times 150 pixel ROI mean spectra of 56 leather samples. The ROI mean spectra of the same type of leather were then averaged to obtain a standard spectrum for each type of leather. The Savitzky–Golay (second-order polynomial with five points) smoothed mean spectra were chosen to reduce the negative impact of noise on the spectral analysis. At the same time, the spectral data near the measurement boundary of the sensor were deleted, and only the spectral data in the range of 960–1650 nm with a high signal-to-noise ratio were retained for subsequent analysis.

2.5. Spectral Feature Parameters

Using hyperspectral imaging systems to identify leather species allows for the qualitative analysis of its composition in terms of hyperspectral profile characteristics. It enables the extraction of spectral feature parameters for quantitative analysis of the spectral profile. The standard spectral feature parameters are the absorption position (P), depth (H), width (W), area (S), symmetry (AA), and absorption index (SAI) of the spectrum. In this study, the absorption position (P), depth (H), width (W), and area (S) of the spectra were selected (Figure 3).

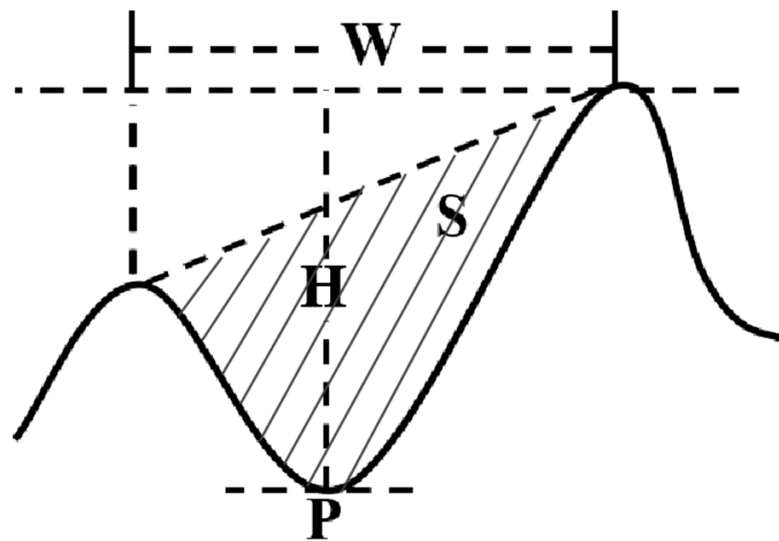


Figure 3. Schematic diagram of the spectral characteristic parameters (the absorption position (P), depth (H), width (W), and area (S)).

Absorption position (P) is the wavelength position corresponding to the lowest reflectance of the absorption valley of the spectral curve. Absorption depth (H) is the distance between the lowest point of the absorption valley reflectance and the highest point of the absorption peak at the shoulder. Absorption width (W) is the spectral bandwidth between the two shoulders of the absorption valley. Absorption area (S) is the area between the lowest reflectivity point of the absorption valley and the two shoulders.

3. Research Results

3.1. Material Composition and Structure

Natural leather is made by processing the dermis layer of animal skin, and only the collagen fibers and the fundamental structural tissue made up of collagen fibers in the dermis layer are retained. Collagen exists in the form of collagen fibers, making it the primary component of natural leather. Collagen is a structural protein with a relative molecular mass of about 300 KDa, with a superhelix structure formed by intertwining three alpha-peptide chains [30]. Like other proteins, collagen has its unique amino acid composition and order of arrangement. The elemental composition of amino acids is an amino group and a carboxyl group attached to the α -carbon atom of the main chain at each end, and a side chain R group and a hydrogen atom attached to the other two ends. The basic structure of amino acids is shown in Figure 4, and the different amino acids only differed in the side chains. Sufficient studies have shown that the amino acid composition and collagen content from different animal sources vary, especially in the imino amino acids (proline and hydroxyproline) [31]. The imino amino acid content of deer skin is approximately 23%, followed by pig skin at approximately 22%, and cattle skin at approximately 21%. Fish collagen has a much lower content of imino acids than mammals, about 15% [32]. Additionally, neither hydroxylysine nor hydroxyproline was found in shark skin.

Regenerated leather is one of the alternatives to natural leather, and the fibers used are leather scraps that have been shredded to a certain extent by grinding machines. In addition, regenerated leather is filled with adhesives such as rubber. A detailed analysis of the component content is not possible due to the intricacy of the sources of natural components and the complexity of creating regenerated leather materials.

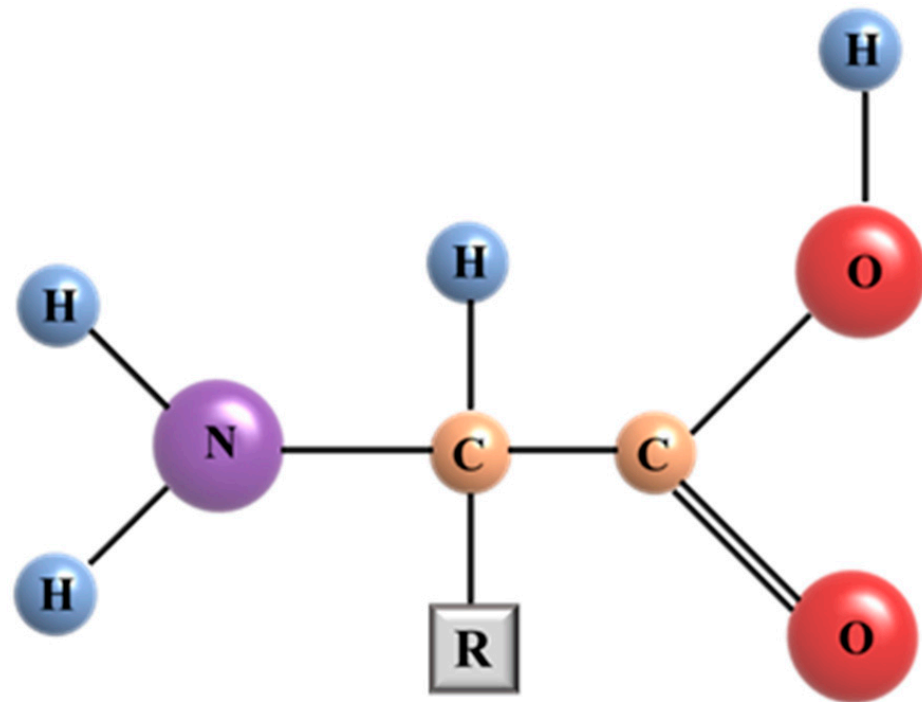


Figure 4. General formula for the structure of amino acids.

SEM was used to provide cross-sectional and fibrous structural characteristics of different leather samples (Figure 5). The structure of natural leather could be divided into a grain layer, a reticular layer, and a flesh layer. Collagen fibers were naturally woven into the structure of each layer in the form of fiber bundles. There was variability in the tightness of the collagen fiber weave of different types of natural leathers, and the percentage of the thickness of the reticular layer had distinct characteristics. Cattle leather was generally thicker, with collagen fibers from the tight mesh layer gradually showing loose characteristics. Sheep leather collagen fibers were woven more closely, and the layered boundary was not noticeable. Pig leather had a prominent layered structure, with thicker collagen fiber bundles in the middle and upper part of the reticulated layer. Deer leather had the most loosely woven collagen fibers compared to other natural leathers. Distinctive scale features could be observed in all cross-sections of the natural leather of reptiles. Lizard leather had a semi-elliptical scale structure in cross-section, and the collagen fibers in the middle of the reticular layer were loosely woven. Snake leather was thin, with a cross-section of obliquely protruding scale structures and an overall oblique delamination boundary. The fibers of crocodile leather were tightly and regularly woven, with subtle cross-sectional scale features and thick fiber bundles in the middle and lower parts near the flesh surface layer. The regenerated leather had no layered structure, the collagen fibers were of varying thicknesses, and the body resembled cardboard. After the mechanical action of the grinder, the collagen fibers in the regenerated leather lost their three-dimensional weave network and were irregularly distributed. Additionally, due to the material used and the processing process of regenerated leather, its fiber bundle edge profile was blurred, and the outline was unclear.

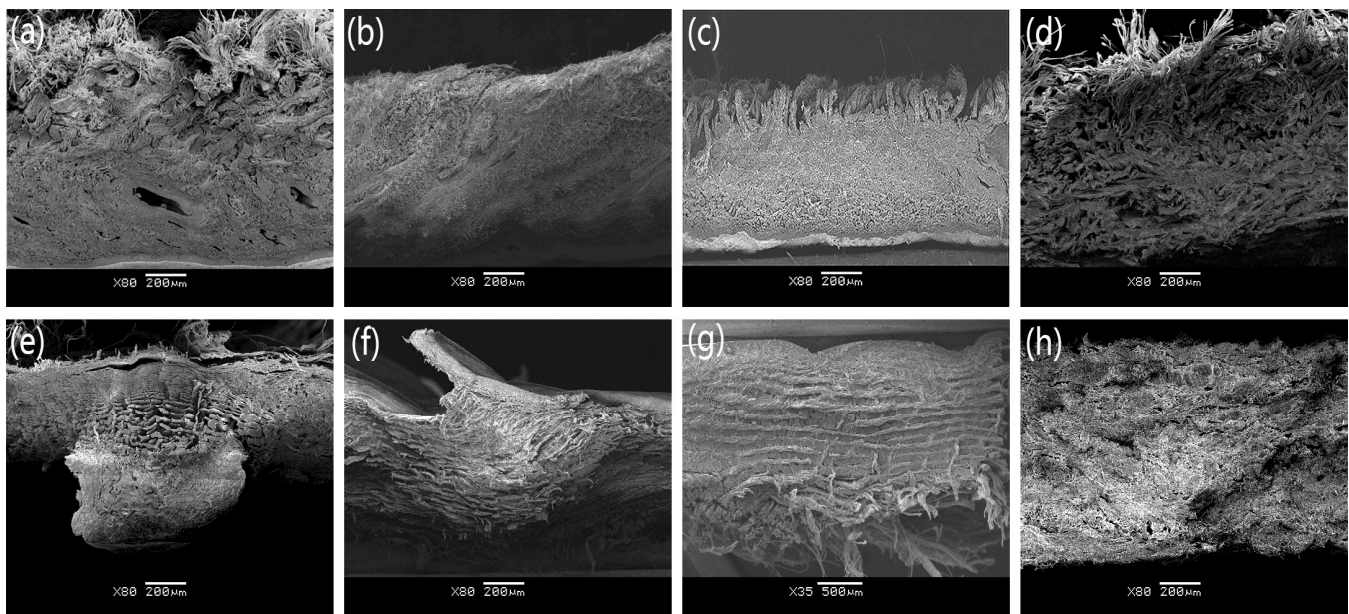


Figure 5. SEM images of (a) cattle, (b) sheep, (c) pig, (d) deer, (e) lizard, (f) snake, (g) crocodile, and (h) regenerated leathers.

3.2. Spectral Characteristics Analysis of Different Kinds of Leathers

The trends in the raw reflectance spectral curves of the mammalian and reptile natural leathers were basically the same (Figure 6). The mammalian and reptilian natural leathers had similar spectral features near 1200 and 1500 nm. The positions of the characteristic peaks were almost identical because their primary components are collagen, whose general structural formula is $R-CH(NH_2)-COOH$ [33]. The absorption features near 1200 nm and 1500 nm originated from the secondary octave absorption of C–H fundamental vibrations and the primary octave absorption of the N–H and O–H stretching vibrations in the proteins, respectively [34]. There were differences in the reflectance of different types of natural leathers, partly due to slight differences in the composition of amino acids in natural leathers from different sources. The process of dyeing and manufacturing leather specimens also affected the reflectance strength of the specimens [35]. At the same time, researchers have also shown that the density of the material weave correlates with the variability in reflectance intensity in the near-infrared region (NIR), with lower weave density materials being able to transmit light better, resulting in lower reflectance [36]. The black deer leather samples had the loosest fiber weave and exhibited a better ability for light absorption, which led to a lower reflectance.

The regenerated leather was made from the edge waste of natural leather reprocessed by adhesives and contained a small number of collagen fibers. As a result, the regenerated leather exhibited spectral characteristics similar to those of the natural leather part, with only weak absorption peaks near 1500 nm and reflectance values all smaller than those of various kinds of natural leathers, except for deer leather. One of the essential pieces of information to identify regenerated leather was that the only distinctive peaks of regenerated leather had a lower absorption depth, width, and area than the characteristic peaks of natural leathers at the same position. The original reflectance spectra of the natural and regenerated leather were analyzed, and the distinguishability between natural and regenerated leathers was demonstrated.

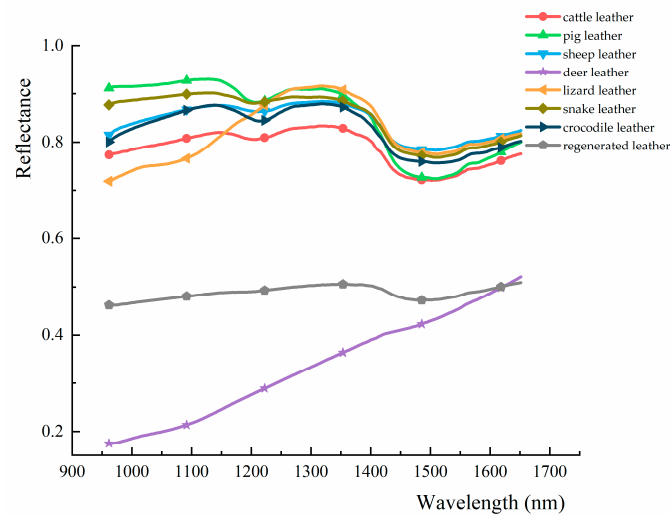


Figure 6. Averaged spectral curves of the regenerated and natural leathers (cattle, sheep, pig, deer, lizard, snake, and crocodile).

3.3. First-Order Derivative Pre-Processing of Hyperspectral Data

From the spectral characteristics of different kinds of leathers, it could be seen that there were some differences in the number, position, intensity, and area of the characteristic peaks of natural leathers and regenerated leather in the range of 960–1650 nm. The classification of regenerated leather could be achieved by comparing the spectral curves with the naked eye. However, the number of characteristic peaks of different kinds of natural leathers in this band range was small, and the difference was slight. Furthermore, it was not easy to achieve the qualitative identification of all kinds of natural leathers only by feature analysis.

Figure 7 shows the raw spectral curves of the seven crocodile leather specimens. Although the positions and numbers of the characteristic peaks of the crocodile leather specimens remained consistent, there were differences in the overall reflectance intensity among the specimens. The phenomenon that the overall reflectance intensity of the identical crocodile leather specimens fluctuated between 0.7 and 0.95 is called “baseline drift”, affecting the accuracy of spectral analysis and subsequent identification models. Therefore, it is necessary to highlight the characteristic differences between different kinds of natural leathers with the help of pre-processing algorithms to establish an identification model with broad applicability and high accuracy.

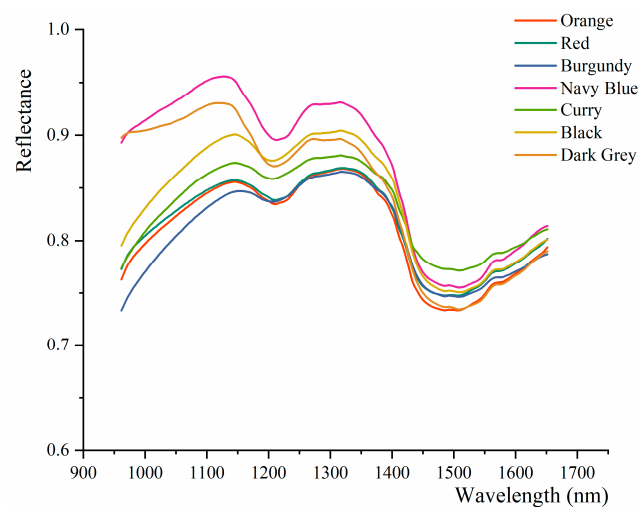


Figure 7. The “baseline drift” phenomenon of the original reflection spectra of the crocodile leather specimens. (Specimens of crocodile leather with different dyeing processes).

In spectral analysis, the first-order derivative is the slope of the tangent line to the curve at each data point, reflecting the rate of change of the original spectral curve. To a certain extent, the spectral data transformed by first-order derivatives can remove the linear and near-linear components from the original data and highlight the inflection and extreme points of the original reflectance curve [37]. The formula for the first-order derivative transformation is as follows:

$$FDR_{(\lambda_i)} = (R_{(\lambda_{i+1})} - R_{(\lambda_i)}) / (\lambda_{i+1} - \lambda_i) \quad (2)$$

where $FDR_{(\lambda_i)}$ is the value of the first-order derivative at wavelength i ; $R_{(\lambda_{i+1})}$, $R_{(\lambda_i)}$ are the reflectance at wavelengths $i + 1$, i , respectively.

These seven kinds of natural leathers produced characteristic peaks in the 1120–1260 nm and 1330–1570 nm wavelength ranges. Moreover, the negative pole point of the first-order derivative value (the point with the fastest rate of decrease of the spectral curve) was generated near 1423 nm (Figure 8). The following analysis could be obtained based on the shape of the curve of the first-order derivative transformed spectrum. In the 960–1650 nm range, the reflection spectrum curve of deer leather increased. Therefore, its first-order derivative value was always positive in this range, and the number of characteristic peaks of the first-order derivative curve was less than that of the other natural leathers. The first-order derivative transformed spectral trend of lizard leather in 1120–1260 nm differed from other leathers, with “convex” characteristic peaks. The snake leather produced a distinct secondary characteristic peak in 1120–1260 nm at 1147 nm. The characteristic peaks of porcine leather in the 960–1650 nm range were most sharply expressed. First-order derivative processing could effectively solve the problem of the “baseline drift” of the original spectrum and more easily recognize different kinds of leathers. The spectral differences of different kinds of leather were highlighted, thus laying a good foundation for further improving the identification accuracy.

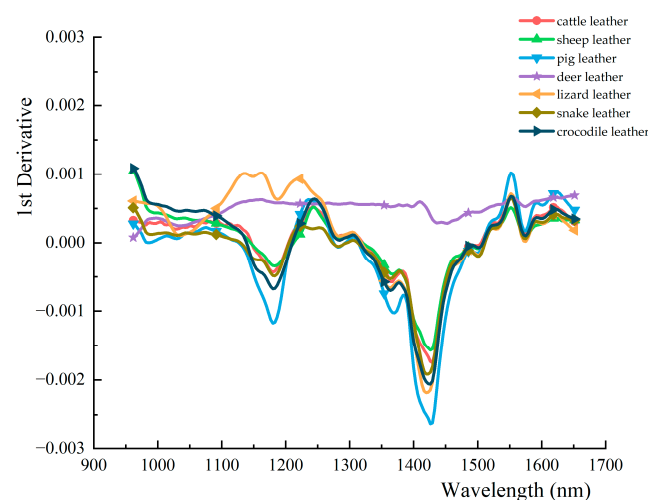


Figure 8. First-order derivative spectra of natural leathers (cattle, sheep, pig, deer, lizard, snake, and crocodile).

3.4. Hyperspectral Data Dimensionality Reduction and Preliminary Classification

Principal component analysis (PCA) is a statistical method that replaces multiple indicators with as few new indicators as representative of the original data and does not overlap [38]. Because the first-order derivative treatment could highlight the spectral differences of different types of leathers more, the first-order derivative transformed spectra of natural leathers were selected for principal component analysis in this study.

The cumulative contribution of the first ten principal components reached 99.9%. There was some overlap in the distribution of the seven different natural leather type ratings on PC1 and PC2. However, the distribution of the seven different types of natural

leathers had patterns when paired with the PC2 and PC3 scores. The distribution of leather varied by quadrant, with sheep leather predominating in the first quadrant, crocodile leather predominating in the second quadrant, pig leather predominating in the third quadrant, and deer leather predominating in the fourth (Figure 9). The distribution of lizard leathers, dispersed in different locations throughout the third quadrant, demonstrated characteristics between the clustered and scattered samples. The scattered distribution of cattle and snake leather might have had some degree of relationship to the selection of the experimental samples because, compared to the other types of leather, the two types used for testing contained the most significant degree of sample possibilities from different manufacturers. Of course, several other types of leather were also combined with samples from different makers with different production processes. According to the score chart, we could obtain a more detailed comparison of the composition content of the seven kinds of natural leathers and achieve a preliminary classification of natural leathers. It replaced the 211 band variables in the hyperspectral data with 10 principal component score variables, compressing the data to the original 4.7%. It both reduced the complexity of the identification model and increased the efficiency of the model operations.

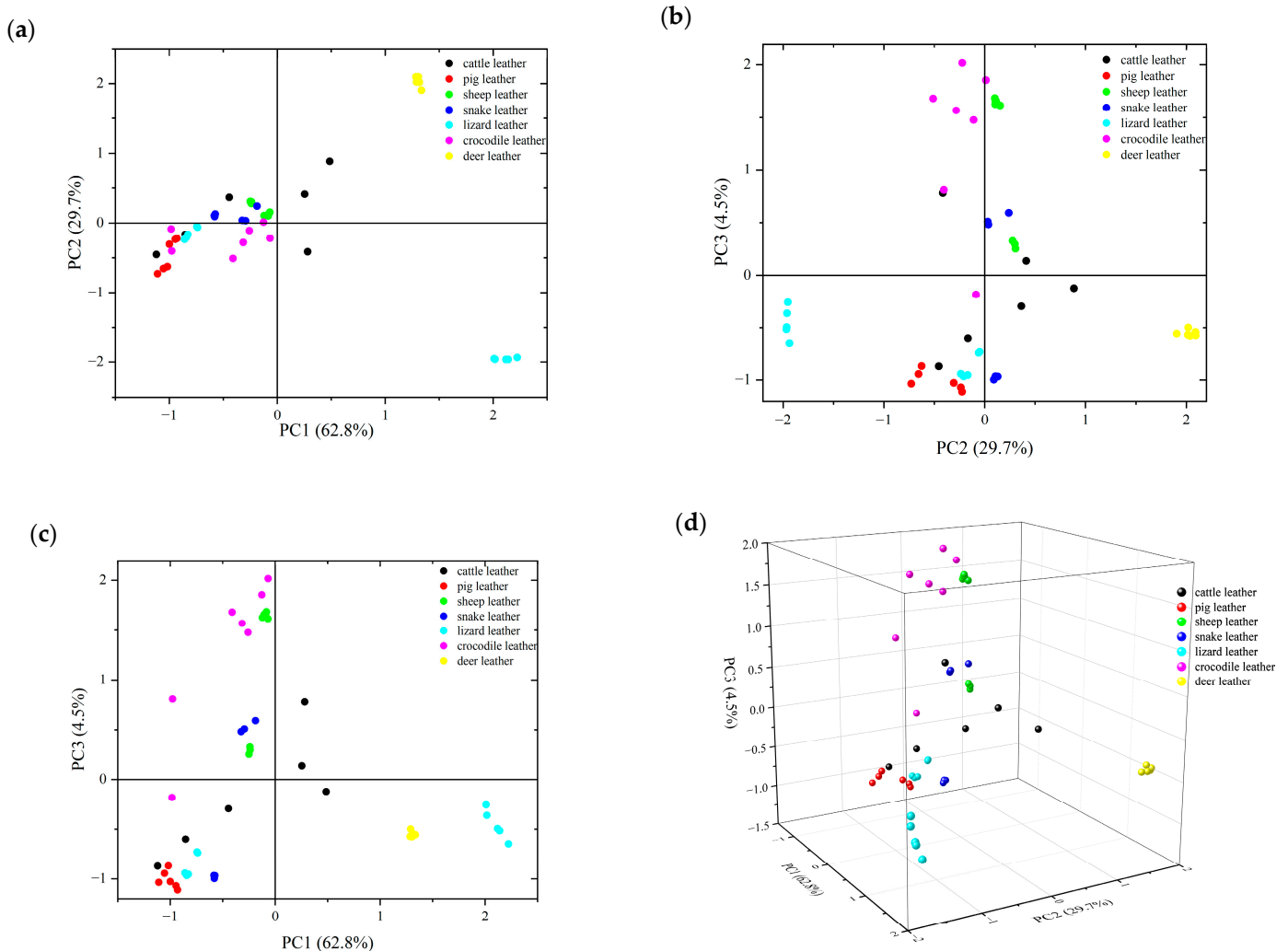


Figure 9. (a) The plot of the natural leather scores on PC1 and PC2; (b) plot of the natural leather scores on PC2 and PC3; (c) plot of the natural leather scores on PC1 and PC3; (d) 3D scatter plot of the principal component scores for natural leathers.

3.5. Establishment and Validation of a Model for the Identification of Natural Leather Species

The content of the natural leather components varied between different species, as shown by the PCA. However, the distribution of the seven different types of natural leather overlapped, and a more suitable aggregation effect was required. Unsupervised principal component analysis (PCA), along with supervised discriminant analysis (DA), has been demonstrated to be an efficient way to lessen the likelihood of over-fitting in pure DA models [39]. The combination of both PCA and DA has achieved good results in other material identification fields, providing a reference for the identification of leather materials. Therefore, we further identified the types of natural leathers with discriminant analysis. The top ten significant component scores for the natural leathers were employed as independent variables. Next, we set values 1 through 7 to the following grouping variables: leather from cattle, sheep, pigs, deer, lizards, snakes, and crocodiles, respectively. In order to conduct a discriminant analysis using the dataset, SPSS software was used to acquire typical discriminant functions and the Bayes classification functions.

According to the model's first six typical discriminant functions and the Wilks' Lambda test results, the classification effect of these six typical discriminant functions for the natural leathers was confirmed to be significant based on p -value less than 0.01 [40]. Among them, the first two discriminant functions cumulatively explained 94.2% of the discriminant model ability, and the correlation coefficients were all greater than 98%. These results illustrate the main contribution of discriminant functions 1 and 2 in identifying the seven natural leather species. The seven types of natural leathers were well clustered on functions 1 and 2 and distributed in different spatial locations, making it easy to identify the species (Figure 10). All leathers of the same animal origin showed good clustering, which shows that the combination of PCA and DA did help to achieve the classification of natural leathers.

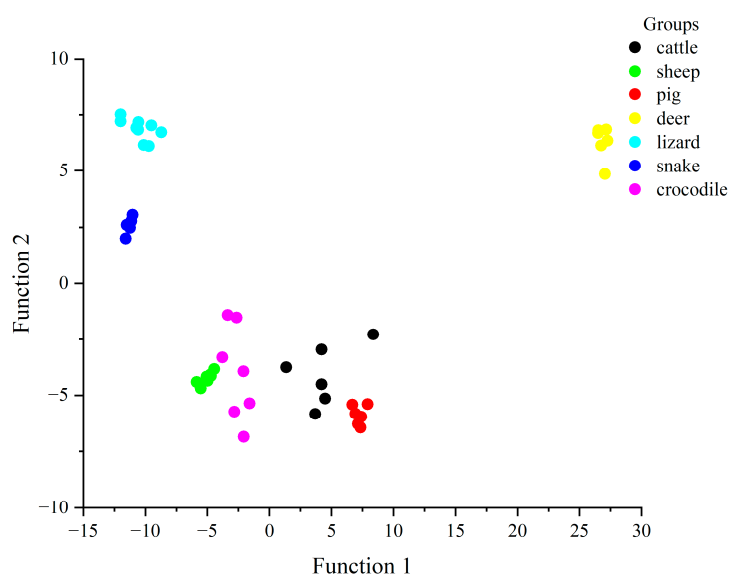


Figure 10. Scatter plot of two typical discriminant function scores for seven types of natural leathers (cattle, sheep, pig, deer, lizard, snake, and crocodile).

The typical discriminant function cannot immediately identify the unknown leather category. Therefore, it was necessary to calculate all of the data (such as the center-of-mass functions for each of the seven types of natural leather samples, the scores of the typical discriminant functions, and the distances between unknown samples and each leather center-of-mass) before establishing the classification criteria for the species. This complex and huge computation is challenging in terms of meeting the efficiency requirements of online testing. However, the direct identification of leather types was made possible by the Bayes classification function, which was produced using discriminant analysis.

Forty-nine spectral data from natural leathers were used as training samples. The discriminant functions of the seven kinds of natural leathers were gained by the method of “first-order derivative—principal component analysis—discriminant analysis”, which are Equations (3)–(9). The discriminative results could be obtained by comparing the magnitude of the function values by substituting the samples of unknown classification into the classification function equations. Whichever classification function had the most considerable calculated value indicated the class of leather to which the piece belonged.

$$\text{Cattle leather: } y_1(x) = -23.988 + 0.274x_1 + 36.375x_2 - 2.133x_3 + 34.965x_4 - 12.816x_5 - 13.41x_6 - 17.563x_7 - 4.116x_8 - 6.276x_9 + 1.864x_{10} \quad (3)$$

$$\text{Sheep leather: } y_2(x) = -29.091 - 25.368x_1 - 40.769x_2 + 28.291x_3 - 31.162x_4 - 0.556x_5 - 0.759x_6 + 1.355x_7 - 7.47x_8 + 7.314x_9 - 4.681x_{10} \quad (4)$$

$$\text{Pig leather: } y_3(x) = -62.809 - 1.802x_1 + 52.61x_2 - 16.3x_3 + 64.294x_4 - 22.306x_5 - 19.998x_6 - 18.337x_7 - 6.16x_8 - 17.856x_9 + 5.604x_{10} \quad (5)$$

$$\text{Deer leather: } y_4(x) = -384.068 + 96.979x_1 + 235.173x_2 - 80.397x_3 + 172.832x_4 - 18.375x_5 - 27.69x_6 - 38.006x_7 + 10.42x_8 - 32.816x_9 + 18.881x_{10} \quad (6)$$

$$\text{Lizard leather: } y_5(x) = -81.477 - 8.741x_1 - 89.215x_2 + 8.814x_3 - 80.624x_4 + 24.759x_5 + 25.382x_6 + 29.445x_7 + 8.735x_8 + 16.21x_9 - 6.14x_{10} \quad (7)$$

$$\text{Snake leather: } y_6(x) = -72.93 - 24.864x_1 - 94.058x_2 + 22.683x_3 - 83.986x_4 + 15.252x_5 + 19.944x_6 + 24.954x_7 + 2.484x_8 + 16.955x_9 - 6.459x_{10} \quad (8)$$

$$\text{Crocodile leather: } y_7(x) = -18.309 - 19.024x_1 - 23.185x_2 + 20.347x_3 - 10.443x_4 - 1.953x_5 - 0.117x_6 - 1.654x_7 - 6.194x_8 + 2.764x_9 - 2.927x_{10} \quad (9)$$

where x_1 – x_{10} represent the scores of the first ten principal components of the first-order derivative spectrum, respectively.

This study tested the classification model established for the seven pieces of natural leather using self-back generation tests and cross-validation. The self-back generation test is a direct prediction validation using training data. Cross-validation, or knife-cutting, divided the data into ten sets. One at a time was selected for the validation set and the remaining nine for the training set, so the validation set had ten possibilities. The model's test classification rate reached 98%, and only one crocodile leather specimen did not receive the correct classification. Furthermore, the cross-validation classification rate of this model was 91.8% correct (shown in Table 1). The overall accuracy of the discriminant model was above 90%, with good prediction results, so it can be practically applied in the identification of natural leather types.

Unlike traditional FTIR spectroscopy, which only acquires spectral information of a single sample at a time, a hyperspectral imaging system can acquire images and the spectral information of multiple samples simultaneously, meeting the basic requirement of fast and efficient online inspection. Even though mass spectrometry, which has emerged in recent years, has made convincing achievements in leather material identification, this method still causes minor damage to the leather samples and is semi-destructive [6,10]. The hyperspectral imaging system used in this study was not limited to the sample size and also avoided the damage caused by the pre-treatment procedure, which did not even cause subsequent routine usage on the experimental sample. Therefore, the method proposed in this study could be used as a non-destructive tool for leather material identification.

Table 1. Classification model validation results for seven types of natural leathers.

Inspection Methods	Types of Natural Leathers	Prediction Team Member Information							Total
		Cattle Leather	Sheep Leather	Pig Leather	Deer Leather	Lizard Leather	Snake Leather	Crocodile Leather	
Back generation test	Cattle leather	6	0	0	0	0	0	0	6
	Sheep leather	0	8	0	0	0	0	0	8
	Pig leather	0	0	6	0	0	0	0	6
	Deer leather	0	0	0	6	0	0	0	6
	Lizard leather	0	0	0	0	10	0	0	10
	Snake leather	0	0	0	0	0	6	0	6
	Crocodile leather	0	1	0	0	0	0	6	7
	Correct rate (%)	100	100	100	100	100	100	85.7	98
Cross-validation	Cattle leather	3	0	2	0	0	0	1	6
	Sheep leather	0	8	0	0	0	0	0	8
	Pig leather	0	0	6	0	0	0	0	6
	Deer leather	0	0	0	6	0	0	0	6
	Lizard leather	0	0	0	0	10	0	0	10
	Snake leather	0	0	0	0	0	6	0	6
	Crocodile leather	0	1	0	0	0	0	6	7
	Correct rate (%)	50	100	100	100	100	100	85.7	91.8

4. Conclusions

This study obtained the standard spectral information of natural and regenerated leathers based on a hyperspectral imaging system. The hyperspectral characteristics of various kinds of leather were analyzed. The results showed that the regenerated and natural leather spectra were distinguishable regarding the location, depth, and area of the characteristic peaks. In contrast, the spectral curves of different kinds of natural leathers had some commonality. This is because the main component of both is collagen. Qualitative identification of all classes of leather needed to be conducted with the help of pre-processing and classification algorithms. First-order derivative pre-processing enabled the correction of the “baseline drift” phenomenon while highlighting the spectral differences of different types of leather. The principal component analysis could extract the top ten indicators carrying 99.9% of the original information and realize the descending and preliminary classification of the natural leather hyperspectral data. The “FD-PCA-DA” model established could better identify the natural leather species, and the correct classification rate reached 98%. This study confirmed that the hyperspectral imaging system could be applied to leather material identification and that the method met the requirements of being non-destructive and an efficient online inspection of batch work. This research is important to protect the rights of leather consumers through scientific and digital approaches by developing the leather testing industry. The leather samples used in this study were highly representative of the types of leather available on the market. These materials are widely used in the textile field and appear in large quantities in the industrial field and even in the art field in display items such as leather paintings and leather books. Future research will concentrate on improving the algorithm to enhance the correct recognition rate and applying the proposed method to identify a broader range of leather materials.

Author Contributions: Conceptualization, C.Z. and Q.H.; Methodology, Q.H.; Software, X.J., Q.H. and Z.Z.; Validation, Q.H.; Formal analysis, Q.H. and J.J.; Investigation, Q.H., Y.Q. and Z.Z.; Resources, C.Z., H.Z., and W.T.; Data curation, Q.H. and Y.Q.; Writing—original draft preparation, Q.H.; Writing—review and editing, X.J. and Q.H.; Supervision, C.Z. and X.J.; Project administration, C.Z. and W.T.; Funding acquisition, C.Z., W.T. and X.J. All authors have read and agreed to the published version of the manuscript.

Funding: This research was funded by the Basic Public Welfare Research Program of Zhejiang Province (LGC22E030001), the Eyas Program Incubation Project of Zhejiang Provincial Administration for Market Regulation (CY2022224), and the Open Fund Project of Clothing Engineering Research Center of Zhejiang Province (2021FZK02).

Institutional Review Board Statement: Not applicable.

Informed Consent Statement: Not applicable.

Data Availability Statement: Not applicable.

Conflicts of Interest: The authors declare no conflict of interest.

References

1. Chen, Z.; Deng, J.; Zhu, Q.; Wang, H.; Chen, Y. A systematic review of machine-vision-based leather surface defect inspection. *Electronics* **2022**, *11*, 2383. [[CrossRef](#)]
2. Sudha, T.B.; Thanikaivelan, P.; Aaron, K.P.; Krishnaraj, K.; Chandrasekaran, B. Comfort, chemical, mechanical, and structural properties of natural and synthetic leathers used for apparel. *J. Appl. Polym. Sci.* **2009**, *114*, 1761–1767. [[CrossRef](#)]
3. Yang, C.; Wang, J.; Li, L. A novel approach for developing high thermal conductive artificial leather by utilizing smart electronic materials. *Text. Res. J.* **2017**, *87*, 816–828. [[CrossRef](#)]
4. Neiva, A.M.; Pereira-Filho, E.R. Evaluation of the chemical composition of synthetic leather using spectroscopy techniques. *Appl. Spectrosc.* **2018**, *72*, 921–932. [[CrossRef](#)]
5. Gao, H.; Lin, J.; Jia, X.; Zhao, Y.; Wang, S.; Bai, H.; Ma, Q. Real-time authentication of animal species origin of leather products using rapid evaporative ionization mass spectrometry and chemometric analysis. *Talanta* **2021**, *225*, 122069. [[CrossRef](#)]
6. Kumazawa, Y.; Hattori, S.; Taga, Y. Semi-nondestructive certification of crocodilian leather by LC–MS detection of collagen marker peptides. *Anal. Chem.* **2019**, *91*, 1796–1800. [[CrossRef](#)] [[PubMed](#)]
7. Meyer, M.; Dietrich, S.; Schulz, H.; Mondschein, A. Comparison of the technical performance of leather, artificial leather, and trendy alternatives. *Coatings* **2021**, *11*, 226. [[CrossRef](#)]
8. Merheb, M.; Vaiedelich, S.; Maniguet, T.; Haenni, C. DNA for species identification in leather: Fraud detection and endangered species protection. *Res. J. Biotechnol.* **2015**, *10*, 65–68.
9. Cantero, R.; Riba, J.-R.; Canals, T.; Izquierdo, L.L.; Iturriaga, H. Characterization of leather finishing by IR spectroscopy and canonical variate analysis. *J. Soc. Leather Technol. Chem.* **2009**, *93*, 12–17.
10. Kumazawa, Y.; Taga, Y.; Iwai, K.; Koyama, Y.-I. A rapid and simple LC-MS method using collagen marker peptides for identification of the animal source of leather. *J. Agric. Food Chem.* **2016**, *64*, 6051–6057. [[CrossRef](#)]
11. Baker, B.W.; Reinholz, A.D.; Espinoza, E.O. Digital near-infrared photography as a tool in forensic snake skin identification. *Herpetolog. J.* **2012**, *22*, 79–82.
12. Varghese, A.; Jain, S.; Prince, A.A.; Jawahar, M. Digital microscopic image sensing and processing for leather species identification. *IEEE Sens. J.* **2020**, *20*, 10045–10056. [[CrossRef](#)]
13. Cortea, I.M.; Ghervase, L.; Ratoiu, L.; Rădvan, R. Application of spectroscopic and hyperspectral imaging techniques for rapid and nondestructive investigation of jewish ritual parchment. *Front. Mater.* **2020**, *7*, 1–14. [[CrossRef](#)]
14. Mogstad, A.A.; Johnsen, G. Spectral characteristics of coralline algae: A multi-instrumental approach, with emphasis on underwater hyperspectral imaging. *Appl. Opt. AO* **2017**, *56*, 9957–9975. [[CrossRef](#)]
15. Kuras, A.; Brell, M.; Rizzi, J.; Burud, I. Hyperspectral and lidar data applied to the urban land cover machine learning and neural-network-based classification: A review. *Remote Sens.* **2021**, *13*, 3393. [[CrossRef](#)]
16. Mukundan, A.; Huang, C.-C.; Men, T.-C.; Lin, F.-C.; Wang, H.-C. Air pollution detection using a novel snap-shot hyperspectral imaging technique. *Sensors* **2022**, *22*, 6231. [[CrossRef](#)] [[PubMed](#)]
17. Jeong, Y.; Yu, J.; Wang, L.; Huynh, H.H.; Kim, H.-C. Monitoring asbestos mine remediation using airborne hyperspectral imaging system: A case study of Jefferson lake mine, US. *Remote Sens.* **2022**, *14*, 5572. [[CrossRef](#)]
18. Abenina, M.I.A.; Maja, J.M.; Cutulle, M.; Melgar, J.C.; Liu, H. Prediction of potassium in peach leaves using hyperspectral imaging and multivariate analysis. *AgriEngineering* **2022**, *4*, 400–413. [[CrossRef](#)]
19. Ban, S.; Liu, W.; Tian, M.; Wang, Q.; Yuan, T.; Chang, Q.; Li, L. Rice leaf chlorophyll content estimation using UAV-based spectral images in different regions. *Agronomy* **2022**, *12*, 2832. [[CrossRef](#)]
20. Lindholm, V.; Raita-Hakola, A.-M.; Annala, L.; Salmivuori, M.; Jeskanen, L.; Saari, H.; Koskenmies, S.; Pitkänen, S.; Pölönen, I.; Isoherranen, K.; et al. Differentiating malignant from benign pigmented or non-pigmented skin tumours—A pilot study on 3D hyperspectral imaging of complex skin surfaces and convolutional neural networks. *J. Clin. Med.* **2022**, *11*, 1914. [[CrossRef](#)]
21. Felli, E.; Cinelli, L.; Bannone, E.; Giannone, F.; Muttillio, E.M.; Barberio, M.; Keller, D.S.; Rodríguez-Luna, M.R.; Okamoto, N.; Collins, T.; et al. Hyperspectral imaging in major hepatectomies: Preliminary results from the ex-machyna trial. *Cancers* **2022**, *14*, 5591. [[CrossRef](#)] [[PubMed](#)]
22. Kumar, R.; Kumar, V.; Sharma, V. Discrimination of various paper types using diffuse reflectance ultraviolet-visible near-infrared (UV-Vis-NIR) spectroscopy: Forensic application to questioned documents. *Appl. Spectrosc.* **2015**, *69*, 714–720. [[CrossRef](#)] [[PubMed](#)]

23. Melit Devassy, B.; George, S.; Nussbaum, P. Unsupervised clustering of hyperspectral paper data using T-SNE. *J. Imaging* **2020**, *6*, 29. [[CrossRef](#)] [[PubMed](#)]
24. Guo, J.; Ying, Y.; Cheng, F.; Kang, Y.; Li, F.; Rao, X. Detection of Foreign Materials on the surface of ginned cotton by hyper-spectral imaging. *Trans. Chin. Soc. Agric. Eng.* **2010**, *26*, 355–360.
25. Mustafic, A.; Jiang, Y.; Li, C. Cotton contamination detection and classification using hyperspectral fluorescence imaging. *Text. Res. J.* **2016**, *86*, 1574–1584. [[CrossRef](#)]
26. Jin, X.; Memon, H.; Tian, W.; Yin, Q.; Zhan, X.; Zhu, C. Spectral characterization and discrimination of synthetic fibers with near-infrared hyperspectral imaging system. *Appl. Opt. AO* **2017**, *56*, 3570–3576. [[CrossRef](#)]
27. Li, J.; Meng, X.; Wang, W.; Xin, B. A novel hyperspectral imaging and modeling method for the component identification of woven fabrics. *Text. Res. J.* **2019**, *89*, 3752–3767. [[CrossRef](#)]
28. Zhang, J.; Liu, Y.; Zhang, X.; Hu, X. Evaluation and consistency calibration of hyperspectral imaging system based on liquid crystal tunable filter for fabric color measurement. *Color Res. Appl.* **2022**, *47*, 401–415. [[CrossRef](#)]
29. Chen, S.Y.; Cheng, Y.C.; Yang, W.L.; Wang, M.Y. Surface defect detection of wet-blue leather using hyperspectral imaging. *IEEE Access* **2021**, *9*, 127685–127702. [[CrossRef](#)]
30. Gelse, K.; Pöschl, E.; Aigner, T. Collagens—Structure, function, and biosynthesis. *Adv. Drug Deliv. Rev.* **2003**, *55*, 1531–1546. [[CrossRef](#)]
31. Burgeson, R.E.; Nimni, M.E. Collagen types. Molecular structure and tissue distribution. *Clin. Orthop. Relat. Res.* **1992**, *282*, 250–272. [[CrossRef](#)]
32. Kittiphattanabawon, P.; Benjakul, S.; Visessanguan, W.; Nagai, T.; Tanaka, M. Characterisation of acid-soluble collagen from skin and bone of bigeye snapper (*Priacanthus tayenus*). *Food Chem.* **2005**, *89*, 363–372. [[CrossRef](#)]
33. Papini, M. Reflectance—Absorptance characteristics of natural fiber surfaces. *Sol. Energy Mater. Sol. Cells* **1993**, *29*, 221–232. [[CrossRef](#)]
34. Burke, M.; Dawson, C.; Allen, C.S.; Brum, J.; Roberts, J.; Krekeler, M.P.S. Reflective spectroscopy investigations of clothing items to support law enforcement, search and rescue, and war crime investigations. *Forensic Sci. Int.* **2019**, *304*, 109945. [[CrossRef](#)]
35. Cai, W.; Xin, W.; Zhang, H.; Luo, Y. Synthesis and application of a low dye absorption waterborne polyurethane for microfiber synthetic leather. *Coatings* **2022**, *12*, 728. [[CrossRef](#)]
36. Haran, T. Short-wave infrared diffuse reflectance of textile materials. *Phys. Astron. Theses* **2008**, *17*, 46–63.
37. Mamedov, I.E.; Suleymanov, T.I.; Ismailov, K.K.; Asadov, H.H. Problems of optimizing preprocessing hyper-spectral data with derivative of the first order. *Proc. Tula States Univ.-Sci. Earth* **2017**, *4*, 60–66.
38. Beattie, J.R.; Esmonde-White, F.W.L. Exploration of principal component analysis: Deriving principal component analysis visually using spectra. *Appl. Spectrosc.* **2021**, *75*, 361–375. [[CrossRef](#)]
39. Wang, H.; Cao, X.; Han, T.; Pei, H.; Ren, H.; Stead, S. A novel methodology for real-time identification of the botanical origins and adulteration of honey by rapid evaporative ionization mass spectrometry. *Food Control.* **2019**, *106*, 106753. [[CrossRef](#)]
40. Volkova, V.M.; Sanina, A.A. Research of the lambda wilks statistic distribution under conditions of violation of basic assumptions in the discriminant function analysis. In Proceedings of the 2014 12th International Conference on Actual Problems of Electronics Instrument Engineering (APEIE), Novosibirsk, Russia, 2–4 October 2014; pp. 548–551.

Disclaimer/Publisher’s Note: The statements, opinions and data contained in all publications are solely those of the individual author(s) and contributor(s) and not of MDPI and/or the editor(s). MDPI and/or the editor(s) disclaim responsibility for any injury to people or property resulting from any ideas, methods, instructions or products referred to in the content.